

Spanwise organization of upstream traveling waves in transonic buffet

D'Aguanno, A.; Schrijer, F. F.J.; van Oudheusden, B. W.

DOI

[10.1063/5.0062729](https://doi.org/10.1063/5.0062729)

Publication date

2021

Document Version

Final published version

Published in

Physics of Fluids

Citation (APA)

D'Aguanno, A., Schrijer, F. F. J., & van Oudheusden, B. W. (2021). Spanwise organization of upstream traveling waves in transonic buffet. *Physics of Fluids*, 33(10), Article 106105. <https://doi.org/10.1063/5.0062729>

Important note

To cite this publication, please use the final published version (if applicable). Please check the document version above.

Copyright

Other than for strictly personal use, it is not permitted to download, forward or distribute the text or part of it, without the consent of the author(s) and/or copyright holder(s), unless the work is under an open content license such as Creative Commons.

Takedown policy

Please contact us and provide details if you believe this document breaches copyrights. We will remove access to the work immediately and investigate your claim.

Green Open Access added to TU Delft Institutional Repository

'You share, we take care!' - Taverne project

<https://www.openaccess.nl/en/you-share-we-take-care>

Otherwise as indicated in the copyright section: the publisher is the copyright holder of this work and the author uses the Dutch legislation to make this work public.


Spanwise organization of upstream traveling waves in transonic buffet

Cite as: Phys. Fluids **33**, 106105 (2021); <https://doi.org/10.1063/5.0062729>

Submitted: 07 July 2021 • Accepted: 16 September 2021 • Published Online: 07 October 2021

 A. D'Aguanno,  F. F. J. Schrijer and  B. W. van Oudheusden

COLLECTIONS

 This paper was selected as Featured



View Online



Export Citation



CrossMark

ARTICLES YOU MAY BE INTERESTED IN

[Deep learning for reduced order modelling and efficient temporal evolution of fluid simulations](#)

Physics of Fluids **33**, 107101 (2021); <https://doi.org/10.1063/5.0062546>

[Propulsive efficiency and efficacy of a pumping sail](#)

Physics of Fluids **33**, 107105 (2021); <https://doi.org/10.1063/5.0065561>

[Experimental insights on the water entry of hydrophobic sphere](#)

Physics of Fluids **33**, 102109 (2021); <https://doi.org/10.1063/5.0063040>

Physics of Fluids

SPECIAL TOPIC: Flow and Acoustics of Unmanned Vehicles

Submit Today!



Spanwise organization of upstream traveling waves in transonic buffet

Cite as: Phys. Fluids **33**, 106105 (2021); doi: [10.1063/5.0062729](https://doi.org/10.1063/5.0062729)

Submitted: 7 July 2021 · Accepted: 16 September 2021 ·

Published Online: 7 October 2021



View Online



Export Citation



CrossMark

A. D'Aguzzo,^{a)}  F. F. J. Schrijer,  and B. W. van Oudheusden 

AFFILIATIONS

Delft University of Technology, Faculty of Aerospace Engineering, Aerodynamics Department, Kluyverweg 2, 2629HS Delft, The Netherlands

^{a)} Author to whom correspondence should be addressed: A.Daguanno@tudelft.nl

ABSTRACT

This experimental study has the objective of providing new insight into the role of upstream traveling waves (UTWs) in the transonic buffet phenomenon, using the background-oriented schlieren (BOS) technique and corroborating the results with particle image velocimetry. The experiments were carried out on the supercritical OAT15A airfoil under transonic conditions, at a Mach number of 0.7, an angle of attack of 3.5° , and a chord-based Reynolds number of 2.6×10^6 . The specific scope of the investigation is the characterization of the spanwise organization of the buffet phenomenon; therefore, the measurements consider a streamwise–spanwise-oriented field of view on the suction side of the airfoil. A particular topic of interest is the propagation and orientation of upstream traveling pressure waves (UTWs) that occur in transonic buffet. The experimental setup used allowed to confirm the two-dimensionality of the velocity field and of the shockwave, but revealed that the UTWs propagate at a non-zero orientation. Processing of the BOS images with two different procedures (normal and differential), has furthermore allowed to extract the frequency and propagation velocity of the UTWs, which have been confirmed to behave as acoustic waves, traveling at the speed of sound relative to the flow. A further analysis has given hints that the strength of the UTWs is modulated during the buffet cycle and, therefore, in support of the feedback-mechanism description of transonic buffet.

Published under an exclusive license by AIP Publishing. <https://doi.org/10.1063/5.0062729>

I. INTRODUCTION

The flight envelope of an aircraft operating at high subsonic velocities is bounded by several limitations—one of those consists in the wing experiencing oscillations of a shockwave on its suction side for a certain range of Mach number (Ma), angle of attack (α), and Reynolds number (Re) (see the review papers of Lee, 2001 and Giannelis *et al.*, 2017). This phenomenon is referred to as transonic buffet and it may ultimately result in violent structural oscillations of the wing, the so-called buffeting, in addition to the oscillations of the aerodynamics loads. The first studies of transonic buffet were undertaken by Hilton and Fowler (1952) while a more complete discussion of the phenomenon was first given by Lee (1990) describing the shock buffet oscillation as being sustained by a feedback mechanism. As part of this mechanism, Lee (1990) described the occurrence of upstream traveling waves (UTWs) and of downstream traveling waves (DTWs), as being responsible for sustaining the shock oscillation. In this description, the shock oscillation is sustained by an interaction between the shock itself and the UTWs, which, depending on the phase in the buffet cycle, force the shock to move either upstream or downstream. Similar conclusions have been reached by the numerical

work of Deck (2005), which considers that the origin of the upstream traveling waves is due to an interaction between the trailing edge shear layer and a sharp trailing edge. The model of Lee (1990) has been updated by a further study of Garnier and Deck (2010), which considered the UTWs to be able to travel along the pressure side too, confirming the previous experimental results of Finke (1975).

Actually, the first author to report the occurrence of upstream propagating pressure waves was Tjeldeman (1977), in a study of the behavior of a transonic flow around an oscillating airfoil. In this study, the presence of a phase delay between the oscillation of the airfoil and the accompanying oscillation of the shockwave was revealed. In addition, through changing the Mach number an almost linear relation between the frequency and the phase lag was found, therefore indicating a fixed time lag between the two oscillations. This time lag was consistent with the time required by changes at the trailing edge to reach the shockwave. Since these waves were considered to be produced in order to satisfy the Kutta condition at the trailing edge, they were called Kutta waves.

In a similar way, also for a fixed airfoil experiencing transonic buffet, there is an oscillation of a shock and with it, of the conditions

at the trailing edge, causing the formation of the previously described pressure waves. However, it is not fully clear where the vortical structures, responsible for the formation of the UTWs, are created, although in the studies of [Jacquin et al. \(2009\)](#) and [Lee \(1990\)](#) it has been proposed that their origin lies at the shock foot.

The main flow features appearing in the feedback loop description are shown in a sketch in [Fig. 1\(a\)](#), where an oscillating shock wave, the downstream propagating disturbances, and the corresponding upstream propagating pressure waves are visualized. These structures are displayed in both a side view of the airfoil [[Fig. 1\(b\)](#)] and for a top view of the suction side of the airfoil [[Fig. 1\(b\)](#)], with the downstream propagating structures omitted in the latter case for simplicity.

A different approach to explain transonic buffet is present in [Crouch et al. \(2009\)](#), where a global stability analysis revealed that buffet occurs when an unstable global mode appears. This description differs from the feedback loop theory, since the shockwave oscillation is considered self-sustained by disturbances created at the shock-foot, which travel in the wall-normal direction and interact with the shock-wave (SW). Thus, this analysis does not include any acoustic feedback from the trailing edge. The quantitative results obtained with this model are able to faithfully reproduce the previously reported experimental data. Similar results are also obtained by the stability analysis of [Sartor et al. \(2015\)](#). This study also showed that unsteady Reynolds-averaged Navier-Stokes (URANS) simulations are capable of describing the main buffet flow features in fair agreement with the detached eddy simulation (DES) discussed by [Deck \(2005\)](#).

The behavior of transonic buffet on swept wings differs from the behavior on airfoils, with oscillations of the shockwave being of lower amplitude in the former case (see [Paladini et al., 2019](#)). In addition, the well-defined frequency peak which is observed in two-dimensional (2D) buffet is substituted by a broadband peak at a Strouhal number (St) increased by a factor which goes from 4 to 7 (from $St = 0.07$ to $St = 0.2-0.6$). [Iovnovich and Raveh \(2015\)](#) have pointed out that, while the buffet behavior does not differ much from the 2D case for low sweep angles, for sweep angles larger than 20° the differences become more substantial. These differences are connected to the presence of convection phenomena which are referred to as buffet cells. These structures consist in the periodic convection of pressure disturbances of alternating sign generated at the wing root (aft of the shock) which then propagate outboard to the wing tip. In [Crouch et al. \(2019\)](#), a three-dimensional (3D) buffet was addressed applying a stability

analysis to swept and unswept wings. In the latter case, in addition to the unsteady mode present for a 2D airfoil, steady spatial modes appear, which in the presence of a sweep angle become unsteady and propagate outboard along the wing. This stability analysis, which has been obtained for infinite wings, has also been extended by [Timme \(2020\)](#) for finite wings.

The study of buffet on swept wings is very relevant because of its possible occurrence in real flight conditions and has been widely studied in the last few years. However, since a complete comprehension of the buffet behavior on an airfoil (or unswept finite wing) is still far from achieved, this study will try to contribute to the understanding of this topic. In the context of the experimental study that is carried out, it is worth mentioning that an unswept finite wing differs from an ideal 2D airfoil in several aspects. In addition to the presence of the previously mentioned stable spatial modes, another important aspect that characterizes a finite unswept wing is the presence of end effects and/or wall interference, which could result in a corner separation or tip vortices. [Iovnovich and Raveh \(2015\)](#) have shown a difference in behavior between an infinite and a finite swept wing, showing that the presence of tip vortices influences the behavior of transonic buffet at the outboard sections, while for more internal sections the classical behavior observed for an infinite swept wing is obtained once again. Similar observations are also present in the numerical study of [Plante et al. \(2017\)](#). The contribution of finite wing effects for an unswept wing and their possible contribution to transonic buffet is instead a topic that has been hardly discussed in literature and requires further investigations. Nevertheless, in the study by [Jacquin et al. \(2009\)](#) it was concluded that possible 3D side walls effects are contained in a region close to the two extremities of the unswept wing.

A detailed experimental characterization of UTWs on an airfoil was carried out by [Hartmann et al. \(2013\)](#), where high-speed stereoparticle image velocimetry (PIV) was used in order to corroborate the findings of [Lee \(1990\)](#). The results confirmed the presence of a feedback loop between the shockwave and the disturbances produced at the trailing edge (where the UTWs are generated). It is stated that the UTWs start reaching the shock in the final phases of its downstream movement, inducing the shock to start moving upstream again. During the upstream movement of the shock, the widened area of separated flow behind it reduces the formation of DTWs and consequently of UTWs; therefore, the shock upstream movement is not sustained by the UTWs interaction anymore and so it stops its

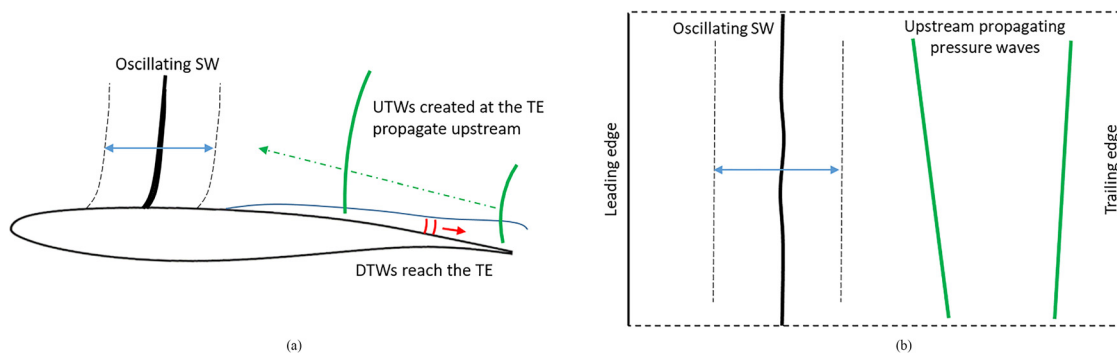


FIG. 1. Sketch of transonic buffet feedback mechanism in a side (a) and in a top view (b).

upstream travel, which closes the feedback mechanism. A similar visualization of upstream propagating pressure waves is also present in Gageik *et al.* (2018) for similar flow conditions on a BAC 3–11 airfoil. In this study, a good agreement of the pressure wave distribution between the numerical and experimental schlieren images is also reported, with a propagation frequency of the pressure waves in the range of 1–2 kHz, similarly to Hartmann *et al.* (2013). In the recent study of Feldhusen-Hoffmann *et al.* (2021), by using dynamic mode decomposition (DMD) a vortex shedding mode with the same characteristic frequency of the UTWs is obtained, supporting the feedback loop description of buffet.

Notwithstanding these observations, there is still no clear consensus in literature whether the UTWs are created only during part of the cycle, or during the whole buffet cycle but with a modulated strength. The difficulties in obtaining this kind of information is associated with the fact that is not easy to detect the UTWs, because as pressure waves, they are relatively weak flow features. An easy and sensitive way of detecting pressure waves is by using the schlieren technique, albeit that the presence of three-dimensionality effects, in particular, in correspondence of the side walls of the wind tunnel, does not permit a clear identification of these waves, as shown in Jacquin *et al.* (2009). On the other hand, a visualization from velocity fields, such as from laser Doppler velocimetry (like in Jacquin *et al.*, 2009) or from particle image velocimetry technique (PIV), does not permit a direct detection of these waves, because of the relatively small velocity fluctuations induced by the pressure waves, as shown in Hartmann *et al.* (2013), where in order to detect these waves it was necessary to apply a high pass filter on the PIV data. Another possibility is using pressure measurements directly on the surface of the airfoil; however, despite the UTWs being produced at the trailing edge, they propagate upstream in the full velocity field and, therefore, cannot be easily detected by pressure measurements at the surface of the airfoil. Jacquin *et al.* (2009), as well, witnessed the difficulty in evaluating the velocity of the UTWs, commenting that more studies on this topic should be accomplished. In contrast, on the pressure side of the airfoil where no relevant flow separation occurs, it was possible to detect structures propagating upstream with a velocity close to the speed of sound relative to the velocity of the flow. In the same work, a cross correlation of the unsteady pressure data on the suction side showed the fluctuations to propagate downstream (DTWs) with a velocity of 17 m/s, which is in agreement with the one obtained by Hartmann *et al.* (2013).

An alternative technique that allows to detect the pressure waves is background-oriented schlieren (BOS), as introduced by Raffel (2015). This technique is based on the same principle of the schlieren technique but does not require optical access from both sides of the wind tunnel, but just from one side. It employs a speckle pattern, which can be directly attached to the model under investigation or used as a background on a wall of the wind tunnel. BOS has been applied in a variety of compressible flow studies, including transonic conditions, like in the work of Klinge *et al.* (2003) where BOS is used together with PIV in order to investigate the wing tip vortex.

In this work, BOS will be used in order to investigate transonic buffet and, in particular, the UTW behavior. To the best of the authors' knowledge, no other application of BOS for detecting UTWs in transonic buffet is present in the literature. By having a direct optical access on the suction side of the airfoil, it has been possible to investigate the spanwise organization of buffet on a 2D airfoil. Similar kinds

of investigations have been reported for 3D wings (like in Dandois, 2016), but not for 2D airfoils. However, despite the general flow field is expected to be 2D, it is still relevant to check whether also particular instantaneous features, such as the UTWs, propagate in a 2D way since they are expected to be caused by structures which propagate in a region where 3D effects are present. The study makes an additional use of PIV to verify the findings from BOS as well as to complement them with the velocity field information.

The organization of the paper is as follows. Section II describes the experimental procedures. In Sec. III, the main characteristics of the shockwave dynamics are documented using experimental results from both BOS and PIV. Later, in Sec. IV, the propagation properties and the strength of the UTWs are obtained using BOS, and they are validated using the PIV data. Finally, Sec. V provides a synthesis of the study, discussing the buffet cycle characteristics based on the results obtained and highlighting the main observations and conclusions.

II. EXPERIMENTAL PROCEDURES

The experimental investigation was carried out in the transonic--supersonic wind tunnel (TST-27) of Delft University of Technology, which is a blowdown wind tunnel with a test section 255 mm high and 280 mm wide. All experiments have been conducted at a total pressure $p_0 = 2$ bar and a total temperature $T_0 = 288$ K. An overview of the main experimental parameters is given in Table I.

A. Model

The model used is the supercritical OAT15A airfoil, with a chord (c) of 100 mm and a span (b) of 200 mm. This airfoil has been designed by ONERA and it has been selected because of its wide use in the studies on transonic buffet both in experimental (Jacquin *et al.*, 2009) and numerical studies (Deck, 2005). In contrast to previous experiments that have been performed in the same wind tunnel (Schrijer *et al.*, 2018, D'Aguanno *et al.*, 2019) for the present investigation, the airfoil was oriented vertically, by mounting it to pylons that are connected to one of the side walls of the tunnel, as shown in Fig. 2(a). The configuration used in this study offers a convenient optical access on the suction side of the airfoil, allowing to study the spanwise organization of the UTWs. In order to ensure a turbulent boundary layer, a full span transition trip with a width of 2% c has been applied at 7% of the chord, using Carborundum 500 particles

TABLE I. Experimental parameters.

| Parameter | Symbol | Value | Units |
|-----------------------------------|-------------|-------------------|-------|
| Free stream Mach number | Ma_∞ | 0.7 | |
| Corrected free stream Mach number | Ma | 0.73 | |
| Free stream velocity | U_∞ | 225 | m/s |
| Total pressure | p_0 | 2 | bar |
| Total temperature | T_0 | 288 | K |
| Chord | c | 0.1 | m |
| Span | b | 0.2 | m |
| Angle of attack | α | 3.5 | ° |
| Thickness to chord ratio | t/c | 12.3 | % |
| Reynolds number based on c | Re_c | 2.6×10^6 | |

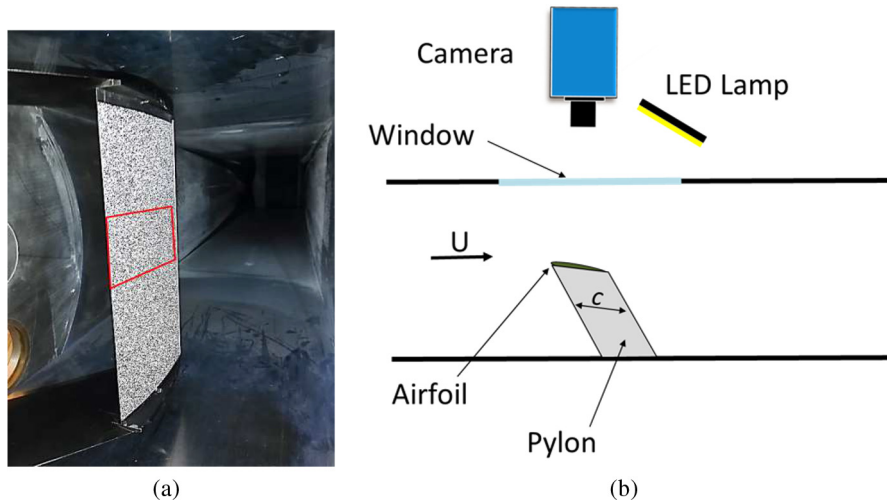


FIG. 2. BOS experimental setup: airfoil with speckle pattern (a) and top view of setup (b).

homogeneously distributed, similar to in the studies of Jacquin *et al.* (2009) and Feldhusen-Hoffmann *et al.* (2018).

The airfoil has been investigated at a free stream Mach number $Ma_\infty = 0.7$ (blockage corrected value $Ma = 0.73$), an angle of attack of $\alpha = 3.5^\circ$, and a chord-based Reynolds number of $Re_c = 2.6 \times 10^6$. These conditions have been selected since previous experiments (Schrijer *et al.*, 2018) showed that shock buffet is fully developed for them.

B. Measurement techniques

To investigate the flow field, two optical techniques were used: background-oriented schlieren (BOS) to investigate the (unsteady) wave pattern and particle image velocimetry (PIV) to capture the instantaneous velocity field.

For the BOS measurements, the surface of the airfoil was covered with a speckle pattern foil as shown in Fig. 2(a). Here, the rectangular area (indicated in red) corresponds to the field of view (FOV) of interest, which ranges from 15% to 100% of the chord (c) in the streamwise direction and from -30% to 30% of c (relative to the mid span

location) in the spanwise direction. The speckle pattern consisted of black synthetic particles printed on a white background, with the particles having a size of 3 to 5 pixels, as suggested by Raffel (2015). The speckle pattern was directly printed on a sheet of paper of 0.09 mm of thickness and attached to the airfoil with glue paint. In order to observe and track the speckle pattern distortion in time, a high-speed camera (Photron Fastcam SA1.1.) was used together with an LED continuous lamp, as shown in Fig. 2(b), which provides a top view sketch of the setup. The acquisition frequency of the camera is 5 kHz, which is sufficient to resolve the shock oscillation in time which occurs at a typical frequency of 160 Hz for this specific airfoil and chord size (Schrijer *et al.*, 2018). The images have been acquired through the camera software PFV (Photron Fastcam Viewer) with a resolution of 1024×640 pixel, and using a 105 mm lens, an f-stop of 2.8 and an exposure time of $15 \mu s$. Thanks to the 8 Gb internal memory of the camera, 8000 images could be stored for each test.

In Fig. 3(a), the setup of the PIV experiment is shown. A Photron Fastcam SA1.1 camera was again used, with an acquisition frequency of 4.65 kHz and a resolution of 1024×640 pixels, with the camera operating in planar PIV mode in order to reconstruct the streamwise

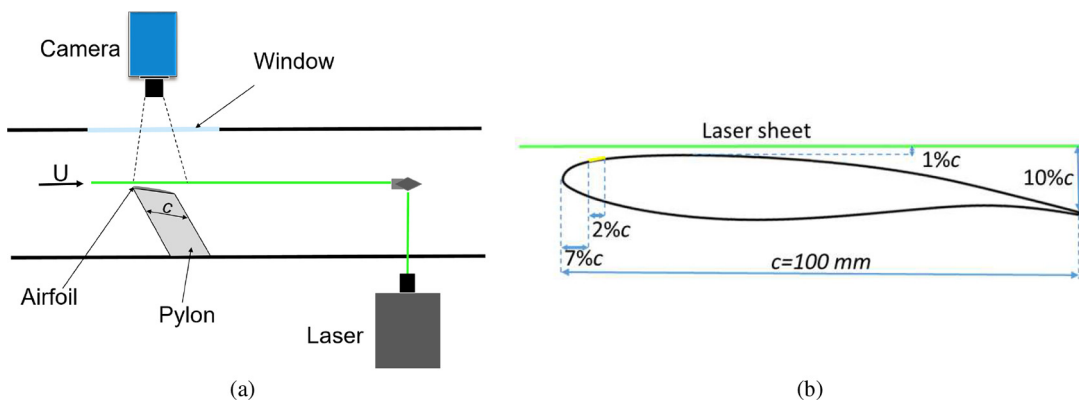


FIG. 3. Top view of PIV setup (a) and detail of laser sheet position with respect to the airfoil (b).

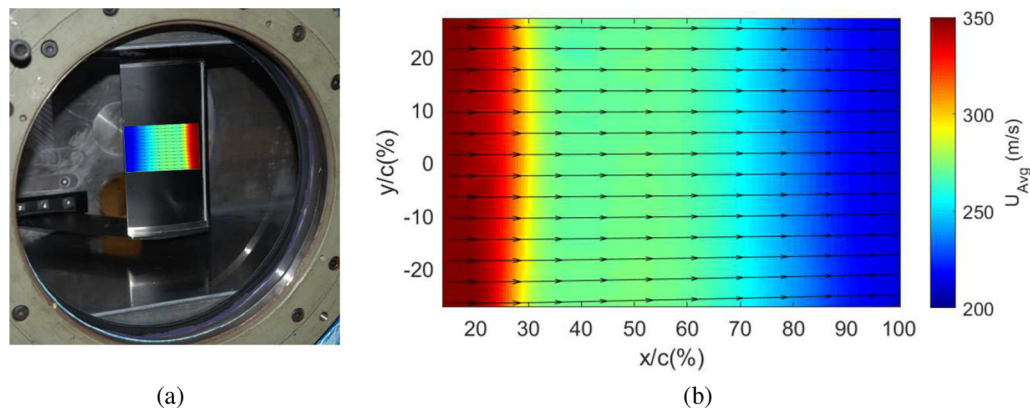


FIG. 4. PIV FOV (a) with corresponding average velocity field (b).

and the spanwise velocity components. Because of the relatively high velocity of the flow ($U_\infty = 225$ m/s), the camera was operated in double pulse configuration ($\Delta t = 3$ μ s), limiting the capacity to 4365 image pairs. The PIV images were obtained by seeding the flow with di(2-ethylhexyl) sebacate (DEHS) particles illuminated with a Mesa PIV dual-cavity high-speed Nd:YAG laser. The laser sheet is parallel to the vertical side walls of the wind tunnel and, therefore, oriented in the direction of the flow, with a thickness of 1.5 mm. As displayed in Fig. 3(b), the area illuminated by the laser is at a non-constant distance from the surface of the airfoil. The laser sheet was located at a distance of 1 mm from the airfoil at its thickest point and at a distance of nearly 10 mm from the surface at the trailing edge. The projection of the FOV on the suction side of the airfoil is similar to the one of BOS, ranging from 15% of the chord to the trailing edge and depicted in Fig. 4(a), where the average velocity field is shown superimposed on the model as well. In the figure also the black foil can be seen, which was applied to the model to reduce the intensity of the laser light reflections.

The PIV data were acquired in the PIV software Davis 8.4.0, which in combination with a high-speed controller was used to synchronize the laser shutter and the exposure time of the camera.

In Fig. 4(b), the average PIV velocity field is given in an enlarged form, confirming that the selected FOV represents part of the fully supersonic area upstream of the shock (between 15 and 25% c) and the subsonic area downstream. Streamlines verify the two-dimensionality of the flow.

C. Data processing

For both the PIV and the BOS measurements, the data have been processed using Davis 8.4.0. For the BOS measurements, first reference images (with the wind tunnel off) were acquired and then the ones in the presence of the flow. Two different processing approaches have been applied to the BOS images. The first is a standard procedure in which each BOS image is correlated with a (no-flow) reference image. The second takes a differential approach in which each image is correlated with the following one (both with the wind tunnel on). In both cases, a multi-pass approach has been chosen for the correlation, using two initial passes with a window size of 64×64 pixels and two subsequent passes with a circular window of 24×24 pixels and an overlap of 75%.

For the PIV measurements, since the raw images were affected by reflections caused by the proximity of the airfoil surface to the laser sheet, first, a minimum subtraction using a Butterworth filter was applied using a filter length of seven images, followed by a cross correlation to obtain the two velocity components. The cross-correlation is computed with the same parameter settings as used for the BOS data, therefore, with two passes of 64×64 pixels and two passes with a final window size of 24×24 pixels and an overlap of 75%. For both BOS and PIV measurements, a resulting vector spacing of 0.55% of the chord was obtained. The main acquisition and processing parameters for PIV and BOS are also reported in Table II.

Further processing for the BOS and PIV data was carried out in *Matlab*.

D. Uncertainty analysis

In this subsection, an estimation of the uncertainty of the experimental results is carried out. The attention is here focused on the sources of error associated with the measurement techniques itself and to the corresponding processing procedures, yielding the error estimates summarized in Table III. Since the cross correlation procedure used for computing the BOS displacement field and for the PIV velocity field is the same, the uncertainties ε_{cc-PIV} and ε_{cc-BOS} are evaluated in the same way (Rajendran *et al.*, 2020). The imaged particle displacement due to density gradient in BOS is much smaller than the seeding particle displacement in PIV. Thus, the former is evaluated with higher accuracy even if it results in higher relative errors (on the order of 2%–3%) with respect to PIV (1%), as shown by Raffel (2015). The PIV

TABLE II. BOS and PIV settings.

| Setting | BOS | PIV |
|-----------------------|-----------------------|-----------------------|
| Acquisition frequency | 5 kHz | 4.65 kHz |
| Number of images | 8000 | 4365 (pairs) |
| Final resolution | 1024×640 pix | 1024×640 pix |
| Vector spacing | 0.55 mm | 0.55 mm |
| Final window size | 24×24 pix | 24×24 pix |
| Window overlap | 75% | 75% |

TABLE III. Uncertainty errors.

| Uncertainty source | Value |
|---|----------------|
| Cross-correlation PIV (ϵ_{cc-PIV}) | ≤ 3.1 m/s |
| Particle slip ($\epsilon_{slip-PIV}$) | ≤ 50 m/s |
| Cross-correlation BOS (ϵ_{cc-BOS}) | ≤ 0.1 pix |
| Line of sight effect BOS ($\epsilon_{sight-BOS}$) | ≤ 1.25 mm |

images, differently from the BOS snapshots, are affected by the particle slip effect ($\epsilon_{slip-PIV}$), which is associated with the seeding particles not being able to truthfully follow the flow field in the case of strong accelerations or decelerations. This effect is particularly important when strong velocity gradients occur, such as in the presence of shockwave (the value reported in Table III refers to this situation). Nevertheless, with BOS there is an uncertainty in the detection of the shock position associated with the density gradients being integrated in the full line of sight, which goes from the camera to the surface of the airfoil. This error can still be quantified as half of the thickness of the shockwave imprint on the BOS image, which is on the order of 1 mm as reported in Table III ($\epsilon_{sight-BOS}$). This value is not as big as the one which could be obtained for a schlieren experiments (like in Jacquin *et al.*, 2009), where strong interactions at the side walls cause the shock to appear even thicker.

III. SHOCKWAVE DYNAMICS

A. Shock position

From the BOS results, it is possible to obtain both qualitative and quantitative information regarding the shock buffet mechanism. In Fig. 5(a), a typical BOS instantaneous result is shown, visualizing the displacement map of the speckle pattern, with the flow oriented from left to right. Two of the main features of buffet are highlighted: the shock wave (SW, which appears at around 30% of the chord) and the presence of UTWs [in Fig. 5(a) two UTWs are observed, at 55 and 75% of the chord, respectively], which are moving from the trailing edge toward the shock position; the remaining regions in the FOV do not present any relevant density gradient. This image has been obtained using the standard processing procedure, by correlating the deformed image of the speckle pattern with the no-flow reference

image. To better visualize the density gradient, in the images the horizontal component of the displacement of the speckle pattern has been depicted. Figure 5(b) shows the same wave pattern one time step later ($\Delta t = 0.2$ ms), revealing an upstream movement of the UTWs and a downstream movement of the shockwave.

Similar features can be obtained from the PIV data, as evident from Figs. 6(a) and 6(b) where two consecutive instantaneous PIV images are shown for the horizontal velocity component. The shockwave is obtained as a strong velocity gradient, whereas the UTW is represented by a small perturbation in the velocity field traveling upstream. For PIV, the shock position was identified by finding the maximum of the gradient of the horizontal velocity, whereas in BOS, the maximum of the displacement map was taken. In both cases, the shock position X_{SW} has been tracked at the mid span ($y/c = 0$) of the airfoil.

In this study, the BOS images have been divided in two bins: one for the upstream shock movement, i.e., when the shock is moving from the trailing edge to the leading edge, and one for the downstream movement (refer to Fig. 7), with the upstream travel covering 3814 images and the downstream travel 4186 (respectively, 47.7% and the 52.3% of the total number of images). This information implies an asymmetry in the buffet cycle, in that the downstream movement takes longer, therefore indicating that the average downstream velocity of the SW is lower. A similar behavior has been obtained for the PIV images where 52.2% of the images are associated with the downstream movement. To further quantify the SW behavior, the distribution of all the BOS instantaneous SW positions is plotted in Fig. 8(a) in terms of the probability density function (pdf) $p(X_{SW}/c)$, using a bin size of 1% of the chord. In Fig. 8(a), the pdf of all the instantaneous images (“all images” in the legend) shows that the region in which the shock is most likely to be found ranges between 25 and 40% of the chord. The figure also contains the pdf of the shock position for both the upstream and downstream movement separately, in all cases the pdf is normalized with respect to the total number of images. The fact that the pdf of the shock position during the downstream movement [yellow line in Fig. 8(a)] appears to be shifted downstream (with respect to the upstream travel) suggests that the SW is moving faster in the first part of its downstream travel. The pdf relative to the upstream movement is instead almost symmetric with respect to the average shock position (32%c).

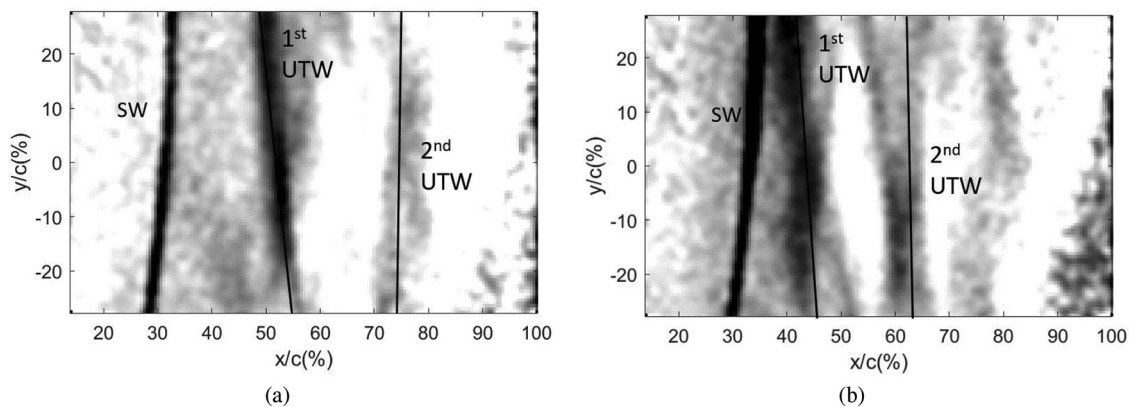


FIG. 5. BOS instantaneous images at time t_0 (a) and $t_1 = t_0 + 0.2$ ms (b).

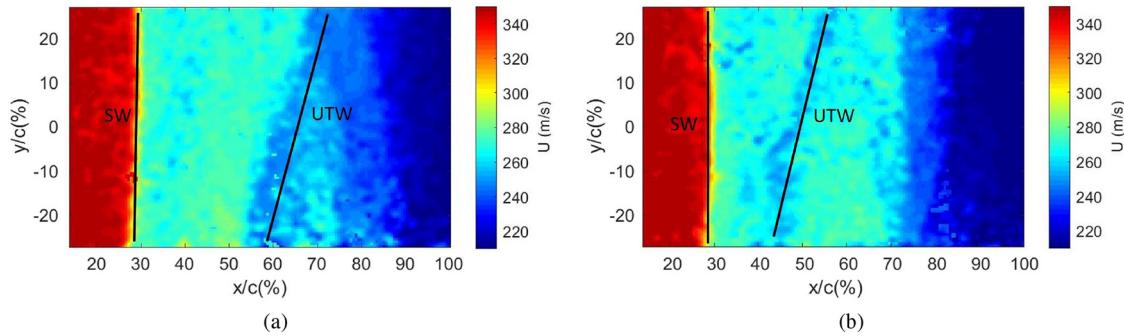


FIG. 6. Instantaneous PIV velocity fields (U) at time t_0 (a) and $t_1 = t_0 + 0.22$ ms (b).

From the information of the shock position in time, the shock velocity has been computed and the relative pdf $p(V_{SW})$ (in this case with a bin size of 1 m/s) is shown in Fig. 8(b). From the pdf, it is clear that the velocity of the shock wave ranges from -20 to 18 m/s, therefore being more likely to have slightly higher velocities during the upstream movement (negative velocities) compared to the downstream movement (positive velocities). As a consequence, average SW velocities of -5.5 and 4.9 m/s are obtained, respectively, for the upstream and downstream travel. This result was expected in view of the lower number of images present in the upstream travel phase with respect to the downstream travel phase.

A similar asymmetry is also documented in Sartor et al. (2015), where the URANS time evolution of the lift coefficient is asymmetric in the two buffet phases with respect to the mean flow value.

B. Spectral analysis

A spectral analysis of the shock location in time has been performed to evaluate the amount of energy associated with the shock oscillation and its main frequency contributions. For this purpose, the

power spectral density (P) associated with the shock position (computed with the Welch method with a procedure similar to the one used by Wang et al., 2020) is plotted in Fig. 9, comparing both BOS (blue line) and PIV (red line).

A good agreement is observed between the PIV and the BOS results over the complete frequency range. It is evident that the main contributions to the shock oscillation are at 160 and 410 Hz. The buffet peak occurs at 160 Hz with a non-dimensional Strouhal number $St = 0.07$ that is very close to the value reported in literature for the same airfoil (in Jacquin et al., 2009, $St = 0.067$). In contrast, the peak present at 410 Hz ($St = 0.172$) is associated with a characteristic frequency of the wind tunnel, which is particularly evident for this experimental configuration. A similar frequency contribution is also observed in Feldhusen-Hoffmann et al. (2018) and attributed to the presence of a cavity in the wind tunnel. An additional broad distribution connected with vibrations of the model is present at around 55 – 70 Hz. An additional peak at 240 Hz is present, with the corresponding physical meaning not being clarified yet.

C. Phase average description

Since buffet is a quasi-periodic phenomenon, the buffet cycle has been subdivided in eight different phases, in order to provide a phase-averaged flow description. The phases are defined according to the shock position and its direction of movement, to distinguish snapshots in which the SW is in the same position, but moving in the opposite direction. According to Fig. 7, in phases 1 and 5, the SW is, respectively, in its most upstream and downstream position. In Table IV, the relative number of images belonging to each phase is reported for both BOS and PIV images. The numbers clearly show that the first and fifth phases contain most images, which is not surprising since those are the two phases in which the shockwave switches direction of motion. Good agreement is present between the two techniques, even if for the BOS data the shock tends to be located more often in the most extreme positions. This difference could be justified by the fact that with BOS all the density gradients are integrated in a direction orthogonal to the surface of the airfoil. Therefore, the resulting BOS images are not able to distinguish between situations in which the shockwave is just changing its inclination (in the streamwise-vertical plane), which is usually happening in correspondence of the turning points in the buffet cycle.

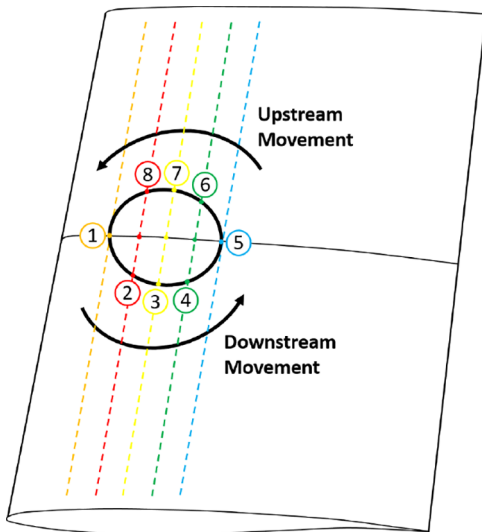


FIG. 7. Sketch of phase definition.

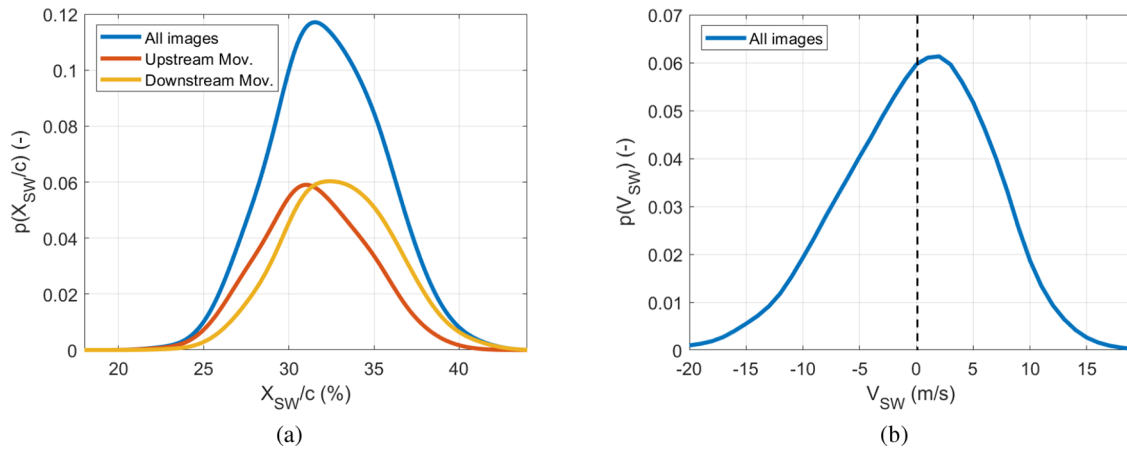


FIG. 8. Pdf of the BOS shock position (a) and velocity (b).

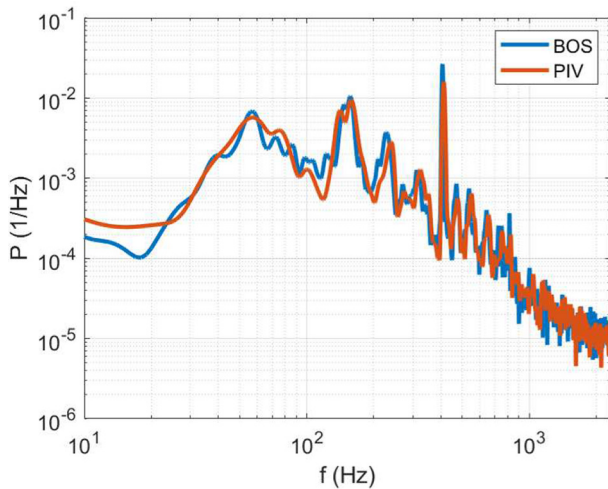


FIG. 9. Psd of the shock position for BOS and PIV data.

Starting from the phase definition, it is convenient to express the PIV velocity field using the so-called triple decomposition,

$$u = u_{avg} + u_{per} + u_{turb}, \tag{1}$$

in which u_{avg} is the mean component of the velocity [shown in Fig. 4(b)], u_{per} is the (quasi-)periodic contribution, and u_{turb} is a quasi-random fluctuating component. The periodic component is obtained

by averaging the PIV processed images belonging to each phase, and subtracting the overall average velocity field. A similar definition of the buffet PIV phases and the associated data processing, applied to a FOV in the streamwise-vertical plane, is given in D’Aguanno *et al.* (2019) where further details can be found.

In Figs. 10(a) and 10(b), the phase-averaged velocity field ($u_{phs} = u_{avg} + u_{per}$) for the horizontal component is shown for the first [Fig. 10(a)] and fifth phases [Fig. 10(b)]. These velocity fields demonstrate that the distance between the shock position in the most downstream and upstream position is approximately 10% of the chord, ranging in locations between 25 and 35% c and, therefore, included in the wider range of oscillation previously shown in Fig. 8(a) for the BOS images. However, it is useful to recall that the amplitude of the shock oscillation is not constant for each cycle, causing the phase-averaged velocity field to be somewhat smoothed out. In addition in a streamwise-vertical plane, the SW is supposed to be almost normal (with respect to the surface of the airfoil) in the most downstream position and more oblique in the most upstream position (see D’Aguanno *et al.*, 2019). Therefore, the projected range of oscillation of the SW in the PIV FOV of this study is reduced with respect to the range in correspondence of the surface of the airfoil.

Although due to the distance of the light sheet from the airfoil surface the separated flow region cannot be observed directly (no reverse flow occurs in the FOV), when taking the low-velocity region as a proxy for this, it can be tentatively concluded that no large difference is present between the two discussed phases, at least not at this distance from the model surface. The velocity fields furthermore confirms that the buffet on a 2D airfoil behaves predominantly as a 2D phenomenon in terms of overall flow features, not having important

TABLE IV. % of images per phase and per technique.

| Technique | Phase 1 | Phase 2 | Phase 3 | Phase 4 | Phase 5 | Phase 6 | Phase 7 | Phase 8 |
|-----------|---------|---------|---------|---------|---------|---------|---------|---------|
| BOS | 20.6 | 9.2 | 10.8 | 9.1 | 21.2 | 10.1 | 9.5 | 9.5 |
| PIV | 16.1 | 9.0 | 11.3 | 11.0 | 16.9 | 13.1 | 12.1 | 10.5 |

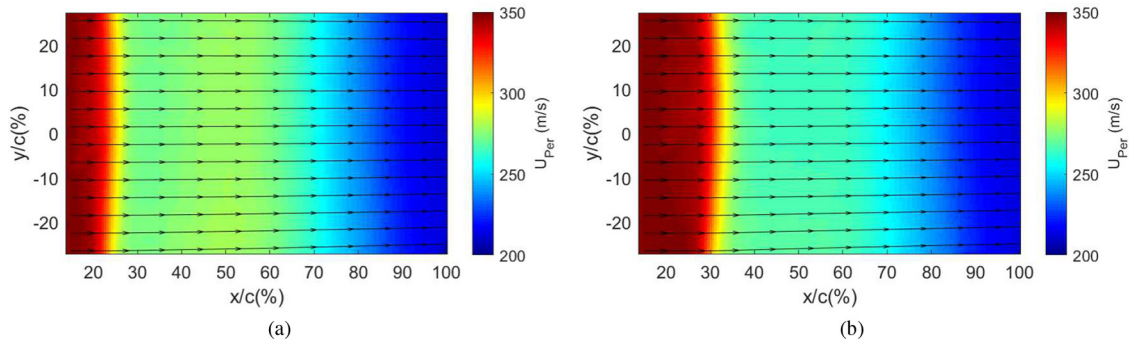


FIG. 10. Phase-averaged velocity field (u component) for the most upstream (a) and downstream shock position (b).

variations in the spanwise direction (both for the shock wave and for the separated area). This applies at least for the imaged region, sufficiently far away from the wing tips, as further confirmed by the nearly parallel orientation of the streamlines (shown for both phases).

IV. UTWS ANALYSIS

A. Detection of UTWs

To detect and characterize the UTWs, the BOS images have been processed using the differential procedure, where the distorted BOS speckle pattern at time step t_0 is cross-correlated with the speckle pattern at the subsequent time step $t_1 = t_0 + \Delta t$ (where $\Delta t = 0.2$ ms), in order to highlight the dynamics of the unsteady flow features. This procedure is similar to what has been referred to as “monoscopic BOS” in the literature, and it is described in more detail by [Bauknecht et al. \(2014\)](#) and [Raffel \(2015\)](#).

The differential BOS result shown in [Fig. 11\(a\)](#) has been obtained using the same images as those to produce the standard BOS images of [Fig. 5\(a\)](#) (t_0) and [Fig. 5\(b\)](#) (t_1). The differential BOS image shows the relative displacement of the speckle pattern between the two successive images. As a result, the image contains the presence of both the shock at time t_0 (in red) and at the following time step ($t_1 = t_0 + 0.2$ ms) (in blue), where the two shockwave signatures appear with opposite sign in the displacement map. The distance between the two imprints represents the distance covered by the shock

within the time separation Δt . Similarly, also the UTWs observed at both the time steps appear in the same image (in red the UTWs corresponding to the first and in blue corresponding to the second time step). It is relevant to consider that this differential method is meaningful only for applications in which the density gradient is moving relative to the field of view and the time between two consecutive images is large enough in order that the density gradients belonging to the two different time steps do not overlap, yet small enough such that the same flow features is present in both images; for the current investigation, both these conditions are satisfied, allowing the UTW behavior to be extracted.

In [Fig. 11\(a\)](#), the UTWs appear sharper in more upstream positions, closer to the shock. In more downstream positions instead, they are less defined due to the masking effect of the separated area.

Each differential image indicates whether the shock is moving upstream or downstream, depending on the relative location of the local maximum and local minimum displacement. The exact distance between the different density features, together with the time separation, allows the computation of the velocity of the shockwave and of the UTWs. In [Fig. 11\(a\)](#), the distance Δx_{UTW} indicates the distance covered by the (first) UTW in one time step and the propagation is considered to be approximately orthogonal to the front of the wave. For the first UTW, a $\Delta x_{UTW}/c = 10\%$ is found; hence, it is propagating upstream with a velocity of nearly $0.01/0.0002 = 50$ m/s

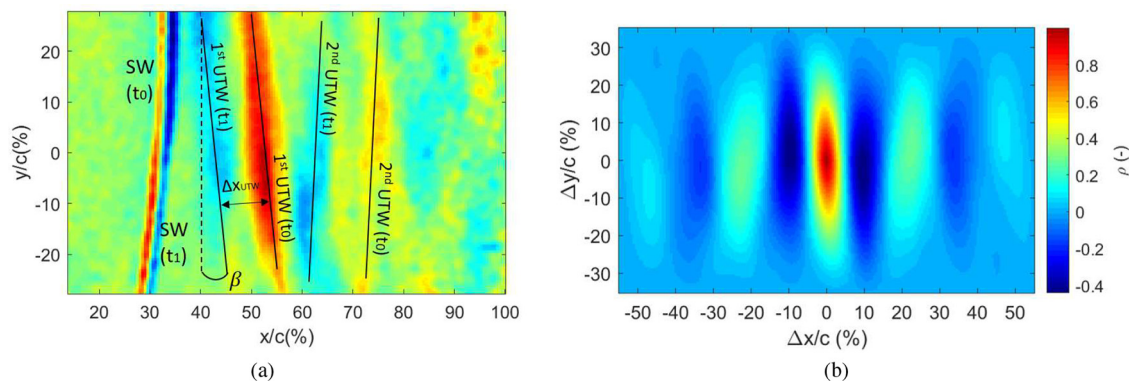


FIG. 11. Instantaneous differential BOS image (a) and corresponding autocorrelation map (b).

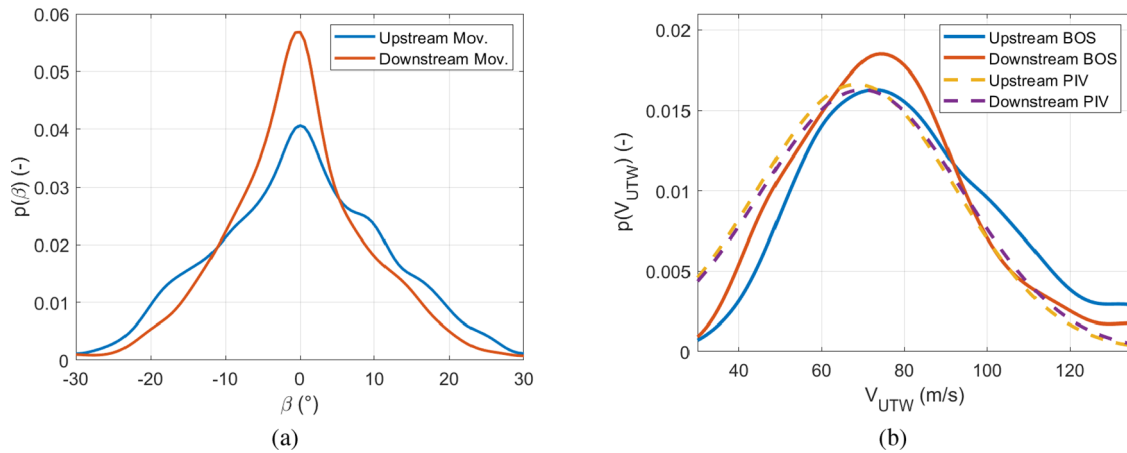


FIG. 12. Pdf of UTW inclination (a) and velocity (b).

$(\Delta x_{UTW}/\Delta t)$ with respect to the flow. From Fig. 11(a), it is further observed that the UTWs propagate with a non-zero angle (β) in the spanwise-streamwise plane, which is similar to what can be observed in Fig. 6(a). For the situation of Fig. 11(a), the first UTW is inclined at an angle $\beta_1 = 6^\circ$, while for the second UTW, this is $\beta_2 = -3^\circ$.

For a systematic detection of the UTWs, an autocorrelation analysis of the displacement field of the differential BOS images was performed. To investigate whether the occurrence of UTWs is associated with just one of the two directions of movement of the shockwave, the upstream and the downstream phases are treated separately. The region in which the autocorrelation is evaluated ranges from 40% to 95% of the chord in the streamwise direction corresponding to the region located downstream of the shock oscillation area, and it extends from -20% to $+20\%$ of the chord in the spanwise direction.

In Fig. 11(b), the instantaneous autocorrelation map corresponding to the differential BOS image of Fig. 11(a) is shown. In the center of the autocorrelation map, there is the main central peak, and both to the right and left of this peak, two negative peaks can be observed ($\Delta x \approx \pm 10$ mm, $\Delta y \approx 0$ mm). The location of the off-center peak corresponds to the distance covered by the UTWs in the time between two consecutive images ($\Delta t = 0.2$ ms). The secondary positive peaks present in the autocorrelation map ($\Delta x \approx \pm 20$ mm, $\Delta y \approx 0$ mm) are instead associated with the distance between the two consecutive UTWs at the same time step.

It is possible to visualize the presence of UTWs also from PIV instantaneous images as shown in Figs. 6(a) and 6(b), where the horizontal component of the velocity field (in the free-stream direction) is shown for two instantaneous consecutive PIV snapshots, with a time interval of 0.22 ms. In these plots, the shock wave is moving upstream, while the UTW at first emerges from the separated area and then moves toward the shock location with a non-zero inclination. Notwithstanding the inclination of the UTW, it is possible to see how the background flow field is nominally 2D, without appreciable changes in velocity in the spanwise direction in both the supersonic and subsonic regions, including the separated (low velocity) area. Between Figs. 6(a) and 6(b), the UTWs is moving upstream of nearly 18% c , thence with a velocity of 82 m/s.

B. Propagation properties of UTWs

In order to obtain the quantitative propagation properties of the UTWs, the autocorrelation procedure described in Sec. IV A was applied to all the images. Although Fig. 11(a) clearly shows the presence of the UTWs, these were not detected in all the images. In order to not contaminate the statistics, all images without UTWs were removed from the ensemble. For this, recordings having a negative peak with $\rho > -0.1$ in the autocorrelation map were discarded. In total, 3708 out of 8000 images were removed.

The correlation maps are analyzed to extract for each time step the inclination (β) and the velocity of the UTWs (V_{UTW}). The results are subsequently sorted, based on the shock motion direction to differentiate between its upstream and downstream movement. The pdf of the UTW inclination $p(\beta)$ is illustrated in Fig. 12(a). The mean value of the inclination of the UTWs is (close to) zero for both the analyzed phases (see Table V) and the pdfs are almost perfectly symmetric with respect to $\beta = 0$. Although the values of inclination range from -25° to $+25^\circ$ in both phases, the pdf is narrower for the downstream compared to the upstream shock movement. This observation results in a higher standard deviation of the inclination of the UTWs for the upstream phase (11.6°) with respect to the downstream movement (9.6°). From a spectral analysis of the value of the UTW inclination in time, no clear peak is observable anywhere in the spectrum, suggesting that the variation of the inclination in time does not change with the buffet frequency and neither is it correlated with the SW position. According to the feedback loop description of buffet, the production of the UTWs is associated with the arrival of vortical structures

TABLE V. UTW properties.

| Property | Upstream Mov. | Downstream Mov. |
|--|---------------|-----------------|
| Mean UTW inclination (β_{avg}) | 0.1° | -0.3° |
| STD of UTW inclination (σ_β) | 11.6° | 9.6° |
| Mean UTW velocity [$(V_{UTW})_{avg}$] | 83.3 m/s | 77.4 m/s |
| STD of UTW velocity ($\sigma_{V_{UTW}}$) | 27.0 m/s | 24.3 m/s |

(DTWs) at the trailing edge. Since the latter structures are highly three-dimensional, the arrival of the DTWs at the trailing edge along the span is not synchronized. This aspect is supposed to be the cause of the non-zero orientation of the UTWs.

An additional explanation of the non-zero inclination of the UTWs could be the presence of corner flow separation at the sides of the airfoil; however, preliminary investigations have excluded this hypothesis. A qualitative visualization of an UTW propagating in the spanwise–streamwise plane with a non-zero inclination is also observed in the numerical study of [Hermes et al. \(2013\)](#) and attributed again to the three-dimensionality of the vortices in proximity of the trailing edge.

Similar to the UTW inclination, the range of velocities of the UTWs is plotted in [Fig. 12\(b\)](#), for both the upstream and downstream shock motion phases. The average UTW velocity obtained during the upstream and downstream travel is, respectively, 83.3 and 77.4 m/s as summarized in [Table V](#), hence obtaining values which are close to those obtained by [Hartmann et al. \(2013\)](#) (80 m/s, under similar experimental conditions). But in addition to what is shown in that study, the pdf of the UTW velocity ($p(V_{UTW})$) shows that there is a wide range of velocities for the UTWs, which varies from 30 to 130 m/s (in terms of absolute values). Pressure waves propagating upstream from the trailing edge of a supercritical airfoil with a similar range of velocities are also observed in the experimental study of [Alshabu and Olivier \(2008\)](#), although for non-buffet conditions. This velocity range can be justified by the assumption that the UTWs, behaving like pressure waves, travel at the speed of sound relative to the flow and therefore with an absolute velocity which differs according to the local velocity of the flow, which is changing with the buffet phase and with the chordwise location. There is a difference in the velocity of the UTWs for the upstream and downstream movement of the shock, with the velocity distribution moved to higher (absolute) values during the upstream shock movement. This result can be understood, considering that during the upstream phase, the separated area is expected to be wider and the flow velocity near the airfoil surface lower ([Jacquin et al., 2009](#)) and therefore, higher velocities for the UTWs are expected.

A detailed evaluation of the UTW velocity for the PIV images is more complicated than for BOS, since in the former case it is not always possible to correctly detect the UTWs because of the relatively low velocity fluctuations accompanying the UTWs. For this reason, in most of the PIV images it was not possible to visualize UTWs. However, starting from the PIV data it has been verified whether the range of velocity of the UTWs obtained with BOS agrees with the assumption that the UTWs propagate at the velocity of sound relatively to the flow. Thus, the local velocity of the UTWs is expressed as the difference between the local velocity and the local speed of sound,

$$U_{UTW} = U_{loc} - a_{loc}. \tag{2}$$

Assuming an ideal gas and the flow to be adiabatic (constant total temperature T_0), the local speed of sound can be expressed in terms of the velocity magnitude $U = \sqrt{u^2 + v^2}$ (with the flow being nominally 2D, the contribution of the out-of-plane velocity component w is not taken into account),

$$a = \sqrt{\gamma RT} = \sqrt{\gamma R \left(T_0 - \frac{U^2}{2c_p} \right)}. \tag{3}$$

Applying this procedure to all the instantaneous images, the theoretical velocity of the UTWs is obtained for each location in the FOV. Restricting the area of interest to a region extending from 40 to 95% in the streamwise direction and from -20 to 20% in the spanwise direction (which is the same area used for the autocorrelation for the BOS images), the normal distribution of the estimated UTW velocity is obtained [[Fig. 12\(b\)](#)]. The range of velocity derived from the PIV flow velocity data matches the BOS experimental results very well (see dashed lines in the plot) confirming the acoustic nature of the UTWs.

The average velocity for the UTWs, estimated with this procedure, is around 70 m/s (in absolute value), which is 10 m/s (or some 15%) lower than the BOS average value. This discrepancy could be justified in view of the distance of the PIV measurement plane from the surface of the airfoil. Hence, the flow is less influenced by the presence of the separated area, bringing to an overestimation of the effective downstream flow velocity and an underestimation of the UTW velocity. This result is confirmed in [Fig. 12\(b\)](#), where the estimated PIV velocity range for the UTWs (dashed lines) is moved to the left (lower velocities) compared to the BOS results (solid lines). Just negligible differences between the upstream and downstream movement are observed for the PIV results, in contrast to the BOS results. This is attributed to the fact that the PIV measurement plane does not capture the pulsation of the separated area, which can be considered responsible for the differences between the upstream and downstream shock motion phases.

Since the velocity of the UTWs changes according to the local velocity of the flow, the non-zero inclination of a UTW is supposed to decrease during its upstream travel (in view of the increase in the local velocity of the flow).

C. Frequency of UTWs

From the average distance between consecutive UTWs, the corresponding propagation frequency can be extracted. To obtain this information, the instantaneous autocorrelation maps are averaged, for the upstream and the downstream shock movement phases separately. In [Fig. 13\(a\)](#), the average autocorrelation map for the downstream movement is shown. In this map, as in the instantaneous one, adjacent to the main central peak ($\Delta x = 0$ mm, $\Delta y = 0$ mm), additional negative and positive peaks occur. Because of the occurrence of a certain amount of variability in the flow field, these additional peaks are smoothed out with respect to those in an instantaneous correlation map. For the same reason, further secondary peaks do not show up in the average map.

The average correlation maps for the upstream and downstream shock movement [which profiles are shown in [Fig. 13\(b\)](#) for $\Delta y = 0$] are very similar and nearly indistinguishable. As no important difference can be discerned between both graphs in [Fig. 13\(b\)](#), this implies that the production of the UTWs occurs very similarly for both phases. From the average autocorrelation map, the average spacing between subsequent UTWs, Δx_{UTW} is obtained as the distance between the central and the secondary positive peaks. Therefore, the average frequency with which the UTWs are produced is estimated (knowing the average velocity of the UTWs, $u_{UTW} = 77.4$ m/s, and the average distance between subsequent UTWs, $\Delta x_{UTW} = 0.32$ c) as

$$f_{UTW} = \frac{u_{UTW}}{\Delta x_{UTW}}. \tag{4}$$

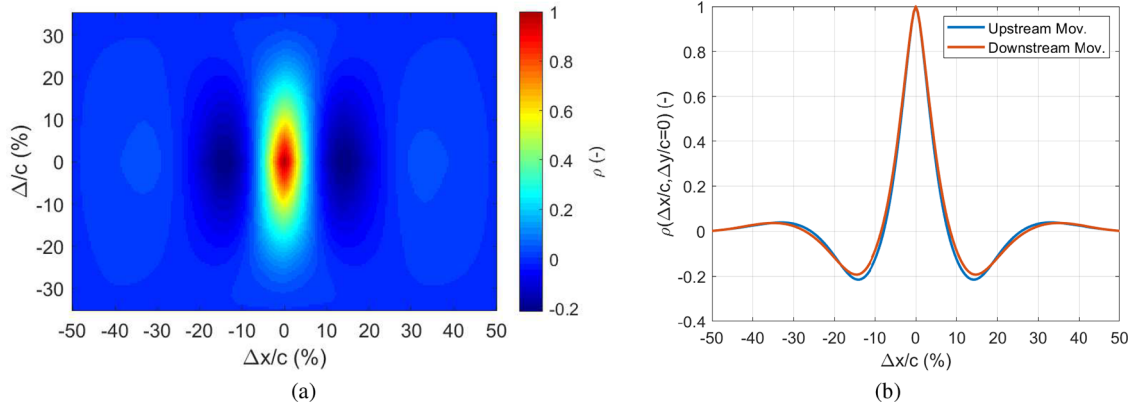


FIG. 13. Average autocorrelation map of the differential BOS images during the downstream movement of the shock (a) and relative profile for $\Delta y/c = 0$ (b).

This frequency is equal to 2400 Hz and corresponds to a Strouhal number of 1.07, which is in good agreement with the value reported by Hartmann *et al.* (2013). It is important to mention that this frequency value is on the limit of the one which could be obtained by a direct spectral analysis of the BOS displacement map given the acquisition frequency of 5 kHz (in view of the Nyquist sampling criterion). However, the procedure used in the present analysis is based on the spatial correlation and is, therefore, not limited by the frequency of acquisition. The symmetry observed in the average autocorrelation map confirms that the UTWs propagate with a zero average inclination value.

D. UTW strength

As anticipated in Sec. IV B, the UTWs are not always clearly detectable in the BOS images. An example of an instantaneous differential BOS image that has been rejected is given in Fig. 14(a), where apart from the presence of the shockwave at both time step t_0 and t_1 , the different UTWs are not unambiguously visualized. The fact that under comparable conditions the UTWs are not easily detectable may

be tentatively associated with a variation in strength of the UTWs. Therefore, the information regarding the relative number of images which have been rejected because of unsatisfactory visualization of the UTWs is used to monitor the production of the UTWs over the buffet cycle. For this purpose, in Fig. 14(b) for each phase in the cycle, as defined in Fig. 7, the ratio of images included in the analysis (R_{incl}) is shown.

For all the phases, the percentage of included images is ranging between 50 and 60% of the relative total number of images for that phase, revealing an increasing trend during the downstream movement, reaching a maximum just before that the shock reaches its most downstream position (phase 5), while decreasing during its upstream travel. This information suggests that UTWs of higher intensity are produced when the shock is close to its most downstream position, with the shock eventually stopping its downstream travel, because of the strong interaction with the UTWs. In contrast, UTWs of lower intensity are produced when the shock is near its most upstream position (phase 1), with the shock not being forced anymore to continue its upstream travel. However, for each phase, the ratio of images in which at least one UTW is detectable is never lower than 50%. This

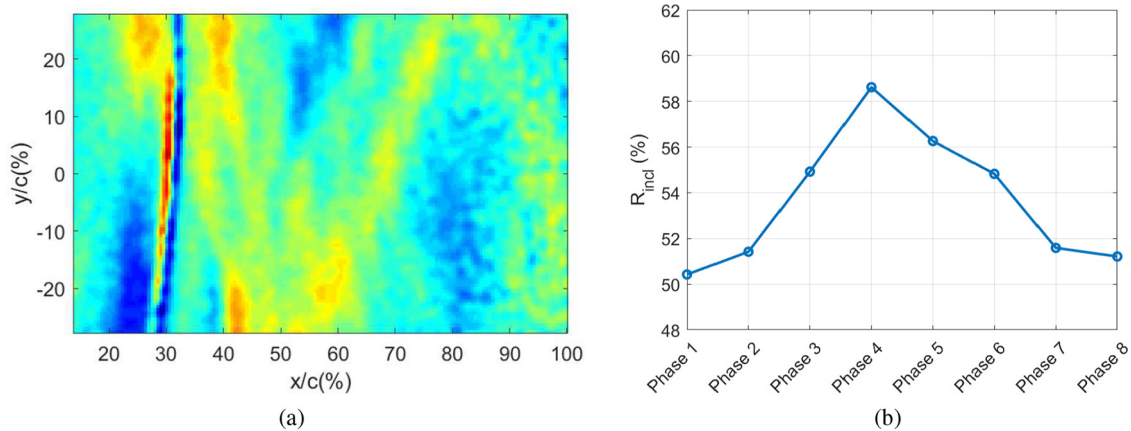


FIG. 14. Analysis of UTW strength variation: example of differential BOS image excluded from autocorrelation analysis (a) and ratio of included images (R_{incl}) per phase (b).

result would suggest that the UTWs are produced along the full buffet cycle, albeit with an intensity, which is modulated according to the phase in the buffet cycle, as theorized by Hartmann *et al.* (2013) and in agreement with the feedback loop description of transonic buffet.

V. CONCLUSIONS

This study has investigated the characteristics of upstream traveling waves (UTWs) in transonic buffet on the OAT15A airfoil using background-oriented schlieren (BOS) and PIV, as main experimental diagnostic techniques. Particular attention has been given on the spanwise organization of the transonic buffet flow features.

The selected orientation of the FOV facilitated an unambiguous analysis of spanwise features, in contrast to the traditional chordwise-vertical plane. In the latter case, the density gradient present in a schlieren image is integrated along the spanwise direction, and therefore, it is heavily affected by edge effects in correspondence of the side walls, where the presence of the developing boundary layer influences the shape of the shockwave and of the other pressure waves present, like in the schlieren data of Jacquin *et al.* (2009) and D'Aguanno *et al.* (2019). Differently, since the pressure gradients are much more coherent along the vertical direction (i.e., normal to the surface of the airfoil), for the streamwise–spanwise FOV less artifacts are introduced in the corresponding BOS image. The simultaneous use of differential BOS has facilitated the analysis of the UTW propagation velocity and demonstrated to be more efficient than PIV in doing so. From the PIV images, only an estimation of the UTW properties could be inferred [Fig. 12(b)], because of the low variation of velocity associated with the UTWs.

The FOV allowed to investigate the two-dimensionality of buffet, which was demonstrated to be strongly coherent along the span of the airfoil both in the supersonic and in the subsonic flow regions (including specific features, such as the SW and the separated area). This evidence was supported by the shape of the shockwave from the BOS images [Fig. 5(a)] as well as by the PIV average results, as shown in Figs. 10(a) and 10(b). In the latter, the streamlines obtained from the two velocity components appear almost completely oriented along the chordwise direction. The shockwave oscillation is observed to occur between the 25 and 40% of the chord of the airfoil [Fig. 8(a)], in both the PIV and the BOS measurements. Notwithstanding the two-dimensional instantaneous organization of the large-scale flow features, it was illustrated that although the average inclination of the UTWs is near zero, they display a non-zero instantaneous angle of inclination in the spanwise–chordwise plane, without important differences between the statistics for the upstream and downstream phases of the buffet cycle [Fig. 12(b)]. This inclination is assumed to be connected with highly three-dimensional structures which upon reaching the trailing edge cause the formation of the UTWs. An additional investigation of these structures from the PIV data was not possible in the current study, because of the distance of the FOV plane with respect to the trailing edge.

By using BOS, it has been further clarified that the propagation velocity of the UTWs is not constant, but ranges between 30 and 130 m/s [Fig. 12(b)], which is consistent with the concept that the UTWs are pressure waves that travel at the speed of sound relative to the local flow. This concept was confirmed by an analysis based on the PIV velocity data. This allows to understand how, as the local flow

velocity changes throughout the buffet cycle, the velocity of the UTWs changes accordingly.

The subdivision of the buffet cycle in an upstream and downstream shock movement phase has confirmed that the UTWs are produced throughout the buffet cycle with a shedding frequency of 2400 Hz, which is in good agreement in terms of Strouhal number ($St = f \cdot c / U_\infty = 1.07$) with Jacquin *et al.* (2009) and Hartmann *et al.* (2013). However, an analysis of the relative number of BOS snapshots in which the UTWs were not perfectly defined suggests that a modulation in the strength of the UTWs is present during the buffet cycle. The results showed that the strongest UTWs are produced when the shock is approaching its most downstream position, forcing the SW to stop its travel and start the upstream movement [see Fig. 14(b)]. Strong UTWs are still reaching the SW in the first part of its upstream movement while they later reduce their strength in the last part of the SW upstream travel. According to literature, the strength of the UTWs is considered to be connected with the strength of vortical structures which when reaching the trailing edge area and passing from a wall bounded shear layer to a free shear layer, are responsible for the production of the UTWs in order to respect the Kutta condition. In view of the current results which show that the UTWs are detected throughout the full buffet cycle, these vortical structures are believed to originate in the separated trailing edge area rather than the shock foot separated area, which is present only in part of the buffet cycle. However, because of the simultaneous pulsation of the shock foot separated area, the strength of these vortices (and as a consequence of the UTWs) is modulated by the former pulsation, which is occurring at the buffet frequency of 160 Hz. These promising results obtained may clarify how a phenomenon which has a propagation frequency of 2400 Hz can influence the buffet dynamics which has a main contribution at 160 Hz, although further study may be required on this matter. Therefore, these results provide evidence that are in agreement with the feedback loop description of transonic buffet.

In synthesis, to clarify the buffet mechanism a full cycle of oscillation is described according to the results obtained in the current investigation and previous findings present in the literature. When the shock starts its downstream travel, its movement is sustained by a region of decreasing pressure at the shock foot, because of the decrease in the extent the separated area. Simultaneously with the reduction of the dimensions of the separated area and shear layer, vortical structures produced in the separated trailing edge area start to be convected downstream. These vortices are relatively strong in this stage, as a large gradient in velocity is occurring over a small region (in these phases the separated area is small as described in Jacquin *et al.*, 2009). When these vortices reach the trailing edge, pressure waves are created that propagate in the full velocity field and communicate with the shockwave along both the pressure and the suction side of the airfoil. The latter reach the shockwave before it arrives in its most downstream position and therefore earlier and with a higher intensity than the UTWs passing through the pressure side. As the pressure behind the UTWs is slightly higher, they require the shockwave to move toward a region with a lower Mach number. This results in a reduction of the velocity of the SW itself and eventually to a stop of its movement. With the further arrival of pressure waves, the shockwave starts its upstream travel, obtaining a velocity of opposite sign with respect to the flow. As a consequence, in this stage, shock foot separation is

triggered, which increases the velocity of the SW even further. With the increase in the extent of the separated area, the vortices, which are responsible for creating the UTWs, become weaker and with them, the strength of the UTWs. This is happening because with the increase in size of the separated area and shear layer, the jump in velocity between the surface of the airfoil and the undisturbed flow is happening in a wider region. In addition, the UTWs traveling in a wide separated area are partly mitigated by this region. The shockwave eventually is not sustained anymore by the increase in pressure due to the presence of the UTWs and stops its upstream travel, which also reduces the size of the separated area. With the beginning of the downstream travel, one full buffet cycle is completed.

Despite further research is still required, this study has provided new insights in a number of aspect related to transonic buffet, in particular, regarding the behavior and spanwise organization of the UTWs. It was furthermore demonstrated that BOS is a very suitable diagnostic technique for the experimental study of transonic buffet.

ACKNOWLEDGMENTS

This work has been carried out as part of the project HOMER (Holistic Optical Metrology for Aero-Elastic Research), funded by the European Commission, program H2020 under Grant No. 769237.

AUTHOR DECLARATIONS

Conflict of Interest

The authors have no conflicts to disclose.

DATA AVAILABILITY

The data that support the findings of this study are available from the corresponding author upon reasonable request.

REFERENCES

- Alshabu, A., and Olivier, H., "Unsteady wave phenomena on a supercritical airfoil," *AIAA J.* **46**, 2066–2073 (2008).
- Bauknecht, A., Merz, C. B., Raffel, M., Landolt, A., and Meier, A., "Blade-tip vortex detection in maneuvering flight using the background-oriented schlieren technique," *J. Aircraft* **51**(6), 2005–2014 (2014).
- Crouch, J. D., Garbaruk, A., Magidov, D., and Jacquin, L., "Global structure of buffeting flow on transonic airfoils," in *IUTAM Symposium on Unsteady Separated Flows and Their Control* (Springer, Dordrecht, The Netherlands, 2009), pp. 297–306.
- Crouch, J. D., Garbaruk, A., and Strelets, M., "Global instability in the onset of transonic-wing buffet," *J. Fluid Mech.* **881**, 3–22 (2019).
- D'Aguzzo, A., Schrijer, F. F. J., and van Oudheusden, B. W., "Transonic buffet control by Means of Upper Gurney Flaps," in Proceedings of the 54th International Conference on Applied Aerodynamics (3AF 2019) (2019).
- Dandois, J., "Experimental study of transonic buffet phenomenon on a 3D swept wing," *Phys. Fluids* **28**, 016101 (2016).
- Deck, S., "Numerical simulation of transonic buffet over a supercritical airfoil," *AIAA J.* **43**, 1556–1566 (2005).
- Feldhusen-Hoffmann, A., Lagemann, C., Loosen, S., Meysonnat, P., Klaas, M., and Schröder, W., "Analysis of transonic buffet using dynamic mode decomposition," *Exp. Fluids* **62**, 66 (2021).
- Feldhusen-Hoffmann, A., Statnikov, V., Klaas, M., and Schröder, W., "Investigation of shock-acoustic-wave interaction in transonic flow," *Exp. Fluids* **59**, 15 (2018).
- Finke, K., "Unsteady shock wave-boundary layer interaction on profiles in transonic flow," AGARD-CP-168 No. 28 (1975).
- Gageik, M., Nies, J., Klioutchnikov, I., and Olivier, H., "Pressure wave damping in transonic airfoil flow by means of micro vortex generators," *Aerosp. Sci. Technol.* **81**, 65–77 (2018).
- Garnier, E., and Deck, S., "Large-eddy simulation of transonic buffet over a supercritical airfoil," in *Direct and Large-Eddy Simulation VII*, edited by V. Armenio, B. Geurts, and J. Fröhlich (Springer, Dordrecht, The Netherlands, 2010), pp. 549–554.
- Giannelis, N. F., Vio, G. A., and Levinski, O., "A review of recent developments in the understanding of transonic shock buffet," *Prog. Aerosp. Sci.* **92**, 39–84 (2017).
- Hartmann, A., Feldhusen, A., and Schröder, W., "On the interaction of shock waves and sound waves in transonic buffet flow," *Phys. Fluids* **25**(2), 026101 (2013).
- Hermes, V., Klioutchnikov, I., and Olivier, H., "Numerical investigation of unsteady wave phenomena for transonic airfoil flow," *Aerosp. Sci. Technol.* **25**, 224–233 (2013).
- Hilton, W. F., and Fowler, R. G., *Photographs of Shock Wave Movement* (ARC R&M, 1952), p. 2692.
- Iovnovich, M., and Raveh, D. E., "Numerical study of shock buffet on three-dimensional wings," *AIAA J.* **53**, 449–463 (2015).
- Jacquin, L., Molton, P., Deck, S., Maury, B., and Soulevant, D., "Experimental study of shock oscillation over a transonic supercritical profile," *AIAA J.* **47**, 1985–1994 (2009).
- Klinge, F., Kirmse, T., and Kompenhans, J., "Application of quantitative background-oriented schlieren (BOS): investigation of a wing tip vortex in a transonic wind tunnel," in Proceedings of the 4th Pacific Symposium on Flow Visualization and Image Processing (PSFVIP-4) (2003).
- Lee, B., "Self-sustained shock oscillations on airfoils at transonic speeds," *Prog. Aerosp. Sci.* **37**, 147–196 (2001).
- Lee, B. H. K., "Transonic buffet on a supercritical aerofoil," *Aeronaut. J.* **94**(935), 143–152 (1990).
- Paladini, E., Dandois, J., Sipp, D., and Robinet, J. C., "Analysis and comparison of transonic buffet phenomenon over several three-dimensional wings," *AIAA J.* **57**, 379–396 (2019).
- Plante, F., Dandois, J., Sartor, F., and Laurendeau, E., "Study of three-dimensional transonic buffet on swept wings," in Proceedings of the AIAA AVIATION Forum (2017).
- Raffel, M., "Background-oriented schlieren (BOS) techniques," *Exp. Fluids* **56**, 60 (2015).
- Rajendran, L., Zhang, J., Bhattacharya, S., Bane, S., and Vlachos, P., "Uncertainty quantification in density estimation from background oriented schlieren (BOS) measurements," *Meas. Sci. Technol.* **31**(5), 054002 (2020).
- Sartor, F., Mettot, C., and Sipp, D., "Stability, receptivity, and sensitivity analyses of buffeting transonic flow over a profile," *AIAA J.* **53**, 1980–1993 (2015).
- Schrijer, F. F. J., Solana Perez, R., and van Oudheusden, B. W., "Investigation of transonic buffet using high speed PIV," in Proceedings of the 5th International Conference on Experimental Fluid Mechanics (ICEFM 2018) (2018).
- Tijdeman, H., "Investigations of the transonic flow around oscillating airfoils," Ph.D. thesis (Delft University of Technology, 1977).
- Timme, S., "Global instability of wing shock-buffet onset," *J. Fluid Mech.* **885**, A37 (2020).
- Wang, Z., Chang, J., Hou, W., and Yu, D., "Low-frequency unsteadiness of shock-wave/boundary-layer interaction in an isolator with background waves," *Phys. Fluids* **32**, 056105 (2020).